An Improved Algorithm for Retrieving Land Surface Emissivity and Temperature From MSG-2/SEVIRI Data

Caixia Gao, Zhao-Liang Li, Shi Qiu, Bohui Tang, Hua Wu, and Xiaoguang Jiang

Abstract—This paper presents an improved algorithm for simultaneously retrieving both land surface emissivity (LSE) and land surface temperature (LST) using data from the Spinning Enhanced Visible and Infrared Imager (SEVIRI) on board the MSG-2 satellite. First, the temperature-independent spectral index-based method for LSE retrieval is reviewed and improved in terms of three aspects: atmospheric correction, fitting of the bidirectional reflectivity model, and retrieval of the LSE in SEVIRI channel 10. Then, the generalized split-window method with seven unknown coefficients is used to derive the LST. Finally, this improved algorithm is applied to several MSG-2/SEVIRI data sets over a study area with geospatial coverage of latitude 30° N–45° N and longitude 15° W–15° E, and using detailed cases, the modifications to the original LSE/LST retrieval methods are shown to be effective and reasonable. In addition, the SEVIRI-derived LSTs are cross-validated primarily using the Moderate Resolution Imaging Spectroradiometer-derived validated LST data extracted from the MOD11B1 product on two clear-sky days (August 22, 2009 and July 3, 2008). The validation results indicate that more than 70% of the differences are within 2.5 K and that the LST differences tend to be lower at night than in the day, which may result from the homogeneous thermal conditions at night.

Index Terms—Cross-validation, land surface emissivity (LSE), land surface temperature (LST), MSG-2/Spinning Enhanced Visible and Infrared Imager (SEVIRI).

C. Gao was with the University of Chinese Academy of Sciences, Beijing 100049, China, and also with ICube, Université de Strasbourg (UdS), Centre National de la Recherche Scientifique (CNRS), 67412 Illkirch, France. She is now with the Academy of Opto-Electronics, Chinese Academy of Sciences, Beijing 100094, China (e-mail: caixiagao2010@hotmail.com).

Z.-L. Li is with the Key Laboratory of Agri-informatics, Ministry of Agriculture/Institute of Agricultural Resources and Regional Planning, Chinese Academy of Agricultural Sciences, Beijing 100081, China, and also with ICube, UdS, CNRS, 67412 Illkirch, France (e-mail: lizl@unistra.fr; lizhaoliang@caas.cn).

S. Qiu is with ICube, UdS, CNRS, 67412 Illkirch, France (e-mail: qtoutou@hotmail.com).

B. Tang and H. Wu are with the Key Laboratory of Resources and Environment Information System, Institute of Geographic Science and Natural Resources Research, Beijing 100101, China (e-mail: tangbh@igsnrr.ac.cn; wuhua@igsnrr.ac.cn).

X. Jiang is with the University of Chinese Academy of Sciences, Beijing 100049, China (e-mail: xgjiang@ucas.ac.cn).

Color versions of one or more of the figures in this paper are available online at http://ieeexplore.ieee.org.

Digital Object Identifier 10.1109/TGRS.2013.2271510

I. INTRODUCTION

LAND surface temperature (LST) is one of the primary factors that govern the energy exchange between the land surface and the atmosphere. This factor is used in global change studies to estimate radiation budgets in heat balance studies and is also a key parameter in climate models [1]. Due to the considerable difficulties of acquiring *in situ* LST representations at the satellite pixel scale, the need for satellite-based LST measurements is highlighted, as these measurements are the only way to provide the LST on a regional or global scale. Therefore, various LST retrieval algorithms have been proposed and developed over the past three decades [2]. These algorithms can be roughly grouped into two categories based on the wavelength used: thermal infrared (TIR) techniques and microwave techniques. However, because of the smaller range in the variation of land surface emissivity (LSE) in the TIR domain and the stronger dependence of the radiance on temperature, there are fewer uncertainties involved in TIR-based LST retrieval than in microwave-based LST retrieval [3]. Therefore, TIR techniques are widely used to estimate the LST from space.

Currently, three major TIR-based LST retrieval methods have been developed, including the single-channel method, the split window (SW) method, and the multiangle method, and all of these methods require *a priori* knowledge of the LSE [2], [4]. The single-channel method retrieves the LST from the radiance measured in a single atmospheric window channel and corrects for atmospheric effects using a confident knowledge of accurate atmospheric profiles [5]. However, these accurate atmospheric profiles are not available with sufficient spatial density or at the same time as the passage of the satellite. The SW method is based on the different atmospheric absorptions in two adjacent channels to correct for atmospheric effects and does not require knowledge of accurate atmospheric profiles. This method was first proposed by McMillin to determine sea surface temperature [6] and extended to LST retrieval by Price [7]. Following the application of this method to LST retrieval, a variety of SW algorithms have been developed and modified with some success to retrieve LST from space instruments such as the Moderate Resolution Imaging Spectroradiometer (MODIS) and Advanced Very High Resolution Radiometer (AVHRR) [2], [8], [9]. The multiangle method is based on a similar principle as that used in the SW method but uses different absorption results from the different atmospheric path lengths that correspond to different observation angles. However, this method assumes that the surface temperature is angular independent.
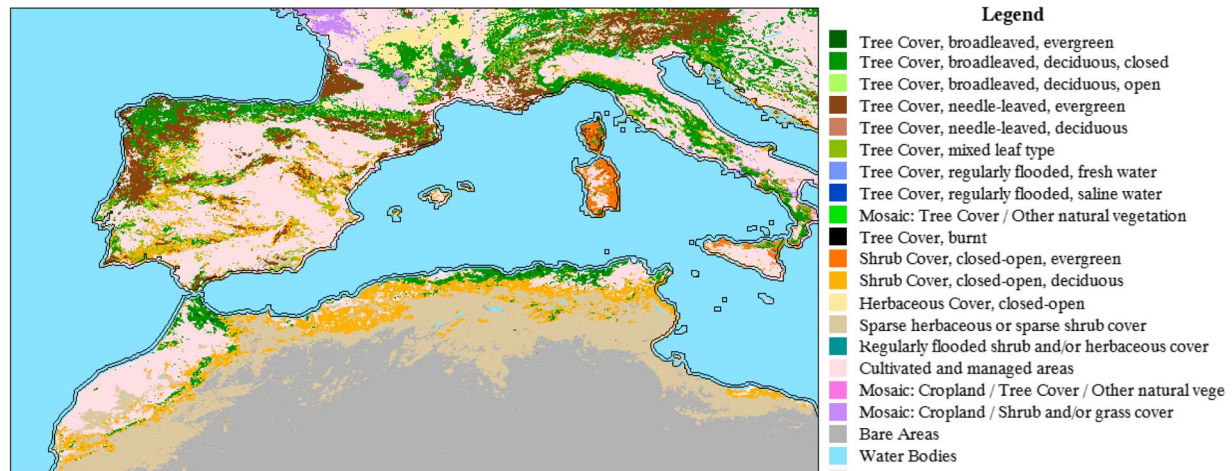
Fig. 1. Land cover of the study area, generated from the Global Land Cover 2000 produced by IES (http://bioval.jrc.ec.europa.eu/products/glc2000/products.php).

The Meteosat Second Generation (MSG) satellite is a new generation of geostationary meteorological satellite (http://www.eumetsat.int). The main payload in this satellite, the Spinning Enhanced Visible and Infrared Imager (SEVIRI), provides data in four visible and near-infrared channels and eight infrared channels every 15 min, which provides the possibility of obtaining the LST more frequently. From these data, a SW method is operationally used to generate an MSG/SEVIRI LST product by the Land Surface Analysis of the Satellite Application Facility (http://landsaf.meteo.pt/). However, the LSE used in this SW method is estimated using the vegetation cover method, which relies on the land cover obtained from land classification maps and on corresponding laboratory measurements of LSE extracted from spectral libraries [10], [11]. Therefore, the accuracy of the retrieved LSE significantly depends on both the accuracy of the land classification and the LSE values assigned to each class [12]. Jiang *et al.* [13] and Jiang [14] estimated the LST from MSG-1/SEVIRI data using a SW method proposed by Becker and Li [15] and improved by Wan and Doizer [8]; in this method, the LSE was derived using the day/night temperature-independent spectral index (TISI)-based method proposed by Becker and Li [16] and improved by Li and Becker [17] and Li *et al.* [18]. This method provides a new approach for retrieving the LSE/LST from SEVIRI data. Nevertheless, there are some deficiencies in the algorithms of these methods, such as the atmospheric correction failures in regions with a late local sunrise time and the sensitivity of the bidirectional reflectivity model to errors in the reflectivities. Therefore, based on the work of Jiang *et al.* [13] and Jiang [14], an improved algorithm for retrieving the LSE and LST from MSG-2/SEVIRI data is developed in this paper. Three components of this algorithm are improved: the atmospheric corrections, the fitting of the bidirectional reflectivity model, and the retrieval of the LSE in channel 10 of the SEVIRI. Furthermore, a preliminary validation of the LST retrieved from SEVIRI data using the improved algorithm is performed with MODIS-derived validated LST data extracted from the V5 MOD11B1 product.

This paper is organized as follows. Section II describes the characteristics of the MSG-2/SEVIRI, the study area, and all

data used in this study. The principles of the LSE and LST retrieval methods and their application to SEVIRI data are detailed in Section III. Section IV presents the preliminary results derived from the MSG-2/SEVIRI data and the results of their cross-validation with the MODIS-derived LST product. The last section is devoted to conclusions.

II. DESCRIPTIONS OF THE STUDY AREA AND ALL DATA SETS USED IN THE STUDY

A. Study Area

A study area covering the Iberian Peninsula and part of the Maghreb with a geospatial coverage of latitude $30°$ N–$45°$ N and longitude $15°$ W–$15°$ E is selected. The Iberian Peninsula is the westernmost section of the European continent located between the Mediterranean Sea and the Atlantic Ocean and occupied by Spain and Portugal. This region is dominated by two major climatic groups, namely, the Oceanic or Western Coastal Maritime to the north and the Mediterranean climate in the southern two-thirds of the peninsula. As displayed in the land use/land cover (LULC) map (see Fig. 1), which was generated from the Global Land Cover 2000 produced by the Institute for Environment and Sustainability (IES), the representative LULC in the Iberian Peninsula typically consists of cultivated and managed areas (approximately 53%), tree cover (approximately 35%), and shrub cover (approximately 9%). The Maghreb is primarily defined by a series of physical geographic features that separate the area from the remainder of Africa. This region includes the Northern African nations of Algeria, Tunisia, and Morocco and is covered by the Sahara desert and the Atlas Mountains. The northern region of the Maghreb in the study area is dominated by shrubs (approximately 9%) and herbaceous plants (approximately 26%), whereas the southern region is dominated by bare soil (approximately 52%). The Maghreb has a Mediterranean climate in the north and an arid climate in the south.

B. MSG-2/SEVIRI Data and Ancillary Data

MSG is a series of four geostationary satellites; the latest satellite, MSG-2, was launched in December 2005. The main

This article has been accepted for inclusion in a future issue of this journal. Content is final as presented, with the exception of pagination.

GAO *et al.*: IMPROVED ALGORITHM FOR RETRIEVING LSE AND LST FROM MSG-2/SEVIRI DATA   3

TABLE I
SPECTRAL CHANNEL CHARACTERISTICS OF THE MSG-2/SEVIRI INSTRUMENT

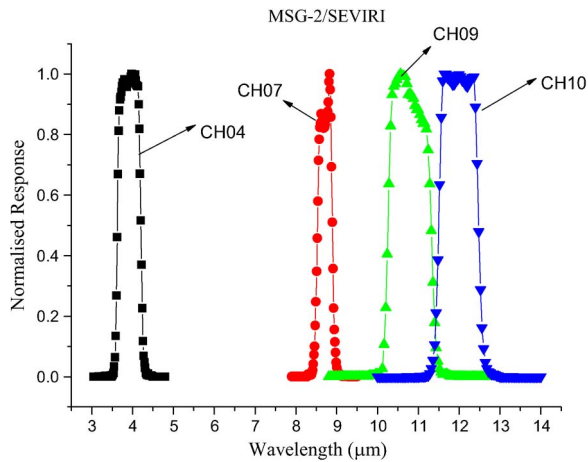| Channel No.	Channel name	Characteristics of spectral channel (µm)			Radiometric error performances	Main gaseous absorber or window
		$\lambda_{central}$	λ_{min}	λ_{max}		
1	VIS0.6	0.65	0.56	0.71	0.27 at 5.3 Wm^{-2}sr^{-1}µm^{-1}	Window
2	VIR0.8	0.81	0.74	0.88	0.21 at 3.6 Wm^{-2}sr^{-1}µm^{-1}	Window
3	NIR1.6	1.64	1.50	1.78	0.07 at 0.75 Wm^{-2}sr^{-1}µm^{-1}	Window
4	IR3.9	3.92	3.48	4.36	0.17 K at 300 K	Window
5	WV6.2	6.25	5.35	7.15	0.21 K at 250 K	Water vapour
6	WV7.3	7.35	6.85	7.85	0.12 K at 250 K	Water vapour
7	IR8.7	8.70	8.30	9.10	0.10 K at 300 K	Window
8	IR9.7	9.66	9.38	9.94	0.29 K at 255 K	Ozone
9	IR10.8	10.8	9.80	11.80	0.11 K at 300 K	Window
10	IR12.0	12.0	11.00	13.00	0.15 K at 300 K	Window
11	IR13.4	13.40	12.40	14.40	0.37 K at 270 K	Carbon dioxide
12	HRV	0.75	Broadband visible		0.63 at 1.3 Wm^{-2}sr^{-1}µm^{-1}	Window/water vapour

Fig. 2.   Normalized spectral response functions for channels 4, 7, 9, and 10 of the SEVIRI.

payload of this satellite, SEVIRI, images an Earth disk with a view zenith angle (VZA) ranging from 0° to 80° and a 3-km nadir spatial resolution and provides data in 12 spectral bands (three visible and near-infrared bands, eight infrared band, and a visible broad-band band; see Table I) every 15 min; it is therefore particularly suited to determining LSE on the day/night TISI concept and then deriving the LST using the SW method. The spectral response functions for channels 4, 7, 9, and 10 of the SEVIRI are shown in Fig. 2.

The primary product of the MSG system is the MSG Level 1.5 product, which can be read by SEVIRI Pre-processing Toolbox (SPT) software. In this paper, to illustrate the improvements on LSE and LST retrievals, the MSG data sets on August 22, 2009, March 13, 2009, July 3, 2008, and March 2, 2008 are used. To delineate all possible occurrences of clouds within each pixel, the corresponding MSG cloud masks are used. In addition, the atmospheric effect for each pixel is corrected using the atmospheric radiative transfer code (MODTRAN 4.0) with the aid of the atmospheric profiles provided by the European Centre for Medium-Range Weather Forecasts (ECMWF). The ECMWF reanalysis operational deterministic model data provide 25-level profiles of pressure, temperature, relative humidity, and geopotential with spatial resolutions of 0.25°/0.25° latitude/longitude at four synoptic coordinated universal time (UTC) times: 00:00, 06:00, 12:00, and 18:00.

Ancillary input data related to the LSE retrieval consists of data on view/sun geometry, digital elevation model (DEM), geolocation information (latitudes and longitudes), and land/sea water mask for each pixel.

Moreover, to acquire the coefficients from simulated data obtained using the SW method for LST retrieval, 1413 clear-sky atmospheric profiles are extracted from the Thermodynamic Initial Guess Retrieval (TIGR) data set (http://ara.lmd.polytechnique.fr/htdocs-public/products/TIGR), which represents a worldwide set of atmospheric situations from polar to tropical atmospheres.

Due to the difficulty of obtaining *in situ* LST measurements at the satellite pixel scale ($\sim$km^2), the MODIS-derived LST over the entire study area, which is extracted from the V5 MOD11B1 product (denoted as MODIS LST), is used to validate the SEVIRI-derived LST in this study. In this paper, the validation is performed with the data on July 3, 2008 and August 22, 2009 to ensure that the validation results are representative, as more valid SEVIRI-derived LST data at different atmospheric and land cover conditions on the two days are available. The MODIS LST product with a spatial resolution of 5.6 km was constructed using the results produced by the day/night LST algorithm and has been validated to have an accuracy greater than 1 K in most cases through field campaigns in 47 clear-sky cases [19], [20]. LSEs from the V5 MOD11B1 product, on the other hand, have not been validated. Therefore, the cross-calibration in this study is carried out in terms of LST. In addition to day and night LSTs for each pixel, information on LSE, VZA, viewing time, and quality control (QC), which are key input parameters for the cross-calibration, is also stored.

Because the LST significantly varies in space and time, this cross-validation of SEVIRI-derived LST with MODIS LST under clear skies (QC = 0) must be conducted on the same site and within as short a time period as possible. Considering the facts that the SEVIRI provides LSTs every 15 min and the SEVIRI measurements closest in viewing time to the MODIS are eligible to be used in this study, only the pixels with a viewing time difference of less than 7.5 min are considered for this cross-validation. In addition, to solve the issue of inconsistency in spatial resolution, a radiance-based pixel aggregation method is employed to match coordinates between the two LST products [14]. Furthermore, because Meteosat is a geostationary meteorological satellite, its sun–satellite viewing geometry results in the observation of sunlit scenes; the MODIS, on the other hand, obtains the LSTs over the entire study area from a wide range of viewing perspectives, and its sun–satellite viewing geometry leads to the detection of a portion of shadow surfaces. To reduce the difference in LST caused by the shadow surfaces, only pixels with MODIS VZAs less than 30° are considered in this study.

All of the data sets used in this study are displayed in Table II.

III. LSE AND LST RETRIEVAL FROM MSG-2/SEVIRI DATA

A. Radiative Transfer Model

Based on the radiative transfer theory, for a clear-sky atmosphere in local thermodynamic equilibrium, the spectral radiance $L(\theta_v, T, \lambda)$ at wavelength λ measured by the sensor at the VZA θ_v can be expressed by the following equations [16]:

$$L(\theta_v, T, \lambda) = R(\theta_v, T_g, \lambda)\tau(\theta_v, \lambda) + R_{atm\uparrow}(\theta_v, \lambda) \quad (1)$$

with

$$R(\theta_v, T_g, \lambda) = \varepsilon(\theta_v, \lambda)B(T_s, \lambda) + (1 - \varepsilon(\theta_v, \lambda))R_{atm\downarrow}(\lambda)$$
$$+ \rho(\theta_v, \theta_s, \varphi, \lambda)E_{sun}(\theta_s, \lambda) \quad (2)$$

TABLE II
DATA SETS USED IN THIS STUDY

	Dataset
	MSG Level 1.5 product
	MSG cloud mask
	ECMWF atmospheric profiles
LSE retrieval	View/Sun geometry data
	DEM data
	Geolocation information
	Land/sea water mask
LST retrieval	TIGR atmospheric profiles
Cross-validation	MODIS LST extracted from V5
	MOD11B1 product

where T is the brightness temperature at the satellite level, T_g is the brightness temperature for surface-leaving radiance, $\varepsilon(\theta_v, \lambda)$ and $\tau(\theta_v, \lambda)$ are the directional spectral emissivity and the total atmospheric spectral transmittance at a VZA of θ_v, respectively, $R_{atm\uparrow}(\theta_v, \lambda)$ is the sum of the upwelling atmospheric spectral radiance and the upwelling diffusion radiance that results from the scattering of solar radiance at a VZA of θ_v, T_s is the LST, $R_{atm\downarrow}(\lambda)$ is the sum of the downwelling hemispheric atmospheric spectral irradiance and the downwelling diffusion irradiance that results from the scattering of solar radiation divided by π, $\rho(\theta_v, \theta_s, \varphi, \lambda)$ is the bidirectional spectral reflectivity, θ_s is the solar zenith angle, φ is the relative azimuth angle between the view azimuth angle and the solar azimuth angle, and $E_{sun}(\theta_s, \lambda)$ is the direct solar spectral irradiance at ground level. For the spectral radiance in the TIR channels and the nighttime measurements in the middle infrared range (MIR) channels, $E_{sun}(\theta_s, \lambda) = 0$, and $R_{atm\uparrow}(\theta_v, \lambda)$ and $R_{atm\downarrow}(\lambda)$ represent only the upwelling atmospheric spectral radiance and the downwelling hemispheric atmospheric spectral irradiance divided by π, respectively.

For a spectral quantity $X(\lambda)$, the measurements in channel i, X_i, can be calculated using the formula

$$X_i = \frac{\int_0^\infty f_i(\lambda)X(\lambda)d\lambda}{\int_0^\infty f_i(\lambda)d\lambda} \quad (3)$$

where $f_i(\lambda)$ is the spectral response function for channel i.

For the channels with a narrow spectral range ($\sim$1.0 μm), the channel-averaged radiance measured in channel i, $L_i(\theta_v, T_i)$, can be expressed using (4) and (5) without introducing significant errors [14]

$$L_i(\theta_v, T_i) = R_i(\theta_v, T_{g,i})\tau_i(\theta_v) + R_{atm\uparrow,i}(\theta_v) \quad (4)$$

with

$$R_i(\theta_v, T_{g,i}) = \varepsilon_i(\theta_v)B_i(T_s) + (1 - \varepsilon_i(\theta_v))R_{atm\downarrow,i}$$
$$+ \rho_i(\theta_v, \theta_s, \varphi)E_{sun,i}(\theta_s). \quad (5)$$

This article has been accepted for inclusion in a future issue of this journal. Content is final as presented, with the exception of pagination.

GAO *et al.*: IMPROVED ALGORITHM FOR RETRIEVING LSE AND LST FROM MSG-2/SEVIRI DATA 5

B. LSE Retrieval

1) Principle of Day/Night TISI-Based Method: This method uses the property that, in the MIR channel (approximately 3.7 μm), the radiance emitted by the land surface itself and the reflected radiance due to solar irradiation during the day are on the same order of magnitude if the surface reflectance in this channel is approximately 0.1 and if there is no solar reflection at night. Li and Becker [17] and Li *et al.* [18] proposed and improved a method to retrieve the LSE using the sun as an active source by defining the two-channel $TISI_{ij}$ without the contribution of solar illumination between channels i and j as (6) through the power-law approximation of Planck's function [12], [13], [21], [22]

$$TISI_{ij} = \left[\frac{R_i(\theta_v, T_{g,i})}{m_i C_i}\right]^{1/n_i} \left[\frac{R_j(\theta_v, T_{g,j})}{m_j C_j}\right]^{-1/n_j} \quad (6)$$

with

$$C_i = \left(1 - \frac{R_{atm\downarrow,i}}{B_i(T_s)}\right) \bigg/ \left(1 - \frac{R_{atm\downarrow,i}}{R_i}\right)$$

where n_i and m_i are the exponents of the power-law approximation of channel radiance: $B_i(T) = m_i T^{n_i}$. The surface temperature T_s involved in the calculation of C_i is approximately calculated as the maximum surface temperature calculated with LSE = 0.98 in channels 7, 9, and 10 since the uncertainties in the estimation of C_i have a minor impact on final results [21].

Assuming that the $TISI_{ij}(i = 4, j = 9$ or $10)$ in the day-time without the contribution of solar illumination is the same as the $TISI_{ij}$ in the nighttime, the bidirectional reflectivity $(\rho_i(\theta_v, \theta_s, \varphi))$ in the MIR channel ($i = 4$ for SEVIRI channel 4) can then be extracted through a comparison of the day and night $TISI_{ij}$

$$\rho_i(\theta_v, \theta_s, \varphi) = \frac{R_i^{day}(\theta_v, T_{g,i})}{E_{sun,i}}$$

$$- \frac{\frac{C^{day}}{C^{night}}\left[\frac{R_j^{day}(\theta_v, T_{g,i})}{R_j^{night}(\theta_v, T_{g,i})}\right]^{n_i/n_j} R_i^{night}(\theta_v, T_{g,i})}{E_{sun,i}} \quad (7)$$

with $C = C_i C_j^{-n_i/n_j}$.

Because the MSG-2/SEVIRI provides data every 15 min with a fixed VZA for a given pixel, various values of $\rho_i(\theta_v, \theta_s, \varphi)$ with different solar illuminated directions during the daytime can be extracted for the same pixel; the LSE in the MIR channel [$\varepsilon_i(\theta)$; see (8)] is then estimated to be a complement to the hemispheric–directional reflectivity, which is the integration of the angular variation of the bidirectional reflectivities described by the RossThick–LiSparse-R model [23], [24]

$$\varepsilon_i(\theta_v) = 1 - \int_0^{2\pi}\int_0^{\pi/2} \rho_i(\theta_v, \theta_s, \varphi) \sin(\theta_s) \cos(\theta_s) d\theta_s d\varphi \quad (8)$$

$$\rho_i(\theta_v, \theta_s, \varphi) = K_{iso,i} + K_{vol,i} \times f_{vol,i}(\theta_v, \theta_s, \varphi)$$

$$+ K_{geo,i} \times f_{geo,i}(\theta_v, \theta_s, \varphi) \quad (9)$$

TABLE III
FITTING PARAMETERS OF THE INTEGRATION OF VOLUMETRIC KERNEL (IF_{vol}) AND GEOMETRIC KERNEL (IF_{geo})

Function	$A_0(B_0)$	$A_1(B_1)$	$t_1(\omega)$ (degree)	θ_c (degree)
$If_{vol}(\theta_v)$	-0.02990	0.01278	21.43823	
$If_{geo}(\theta_v)$	-2.01124	-29.40855	68.81710	90.95449

where $K_{iso,i}$ is the isotropic scattering term in channel i, $K_{vol,i}$ and $K_{geo,i}$ are the coefficients of the volumetric kernel $f_{vol,i}$ and the geometric kernel $f_{geo,i}$ in channel i, respectively.

Assuming that the ratio of the vertical radius to the horizontal width of the spheroid crown is equal to unity and that the distance to the center of the crown above the ground is equal to the vertical radius, for a given VZA ranging from 0° to 80°, Jiang [14] calculated the integration of $f_{vol,i}$ and $f_{geo,i}$ ($If_{vol,i}$ and $If_{geo,i}$) with a step of 0.05° for both the solar zenith angle and the solar azimuth and observed that the exponential growth function [see (10)] and the Gauss function [see (11)] provided very good fits to $If_{vol,i}$ and $If_{geo,i}$, respectively. The fitting parameters of (10) and (11) are shown in Table III

$$If_{vol,i}(\theta_v) = \int_0^{2\pi}\int_0^{\pi/2} f_{i,vol}(\theta_v, \theta_s, \varphi) \sin(\theta_s) \cos(\theta_s) d\theta_s d\varphi$$

$$= A_0 + A_1 \exp(\theta_v/t_1) \quad (10)$$

$$If_{geo,i}(\theta_v) = \int_0^{2\pi}\int_0^{\pi/2} f_{i,geo}(\theta_v, \theta_s, \varphi) \sin(\theta_s) \cos(\theta_s) d\theta_s d\varphi$$

$$= B_0 + \frac{B_1}{\omega\sqrt{\pi/2}} \exp\left[-2\left(\frac{\theta_v - \theta_c}{\omega}\right)^2\right]. \quad (11)$$

Finally, the LSE in the TIR channel ($j = 9$ and 10 for SEVIRI channels 9 and 10), $\varepsilon_j(\theta_v)$, can be derived from

$$\varepsilon_j(\theta_v) = \frac{\varepsilon_i(\theta_v)^{n_i/n_j}}{TISI_{i,j}^{night}}. \quad (12)$$

2) Atmospheric Corrections: It is worth noting that the TISI-based method requires the quantity $R_i(\theta_v, Tg, i)$ ($i = 4, 9, 10$) to construct the TISI and that atmospheric corrections must be performed for the SEVIRI MIR and TIR channels. In this paper, after data checking, cloud screening, and land/sea water masking procedures, the atmospheric correction is performed using MODTRAN 4.0 with ECMWF atmospheric profile data, as the TISI-based method is not sensitive to the error of atmospheric correction. However, because ECMWF atmospheric profiles have lower temporal and spatial resolutions than the SEVIRI data, modified schemes are used to approach this problem. At each synoptic time, the spatial bilinear interpolation method is used to interpolate the atmospheric quantities

estimated with the ECMWF atmospheric profile data using MODTRAN 4.0, and these interpolated atmospheric quantities are then used to correct for the atmospheric effects for SEVIRI pixels. For the data measured at times other than the synoptic time, different schemes are employed to correct for the atmospheric effects in the MIR and TIR channels.

For the MIR channel (SEVIRI channel 4), time-nearest atmospheric quantities are used to correct for atmospheric effects because the measurements in this channel are less sensitive to changes in the atmospheric water vapor content (WVC). However, because SEVIRI channel 4 cannot be regarded as a channel with a narrow spectral range, the use of (4) will introduce large errors in the radiance at ground level in this channel. Jiang et al. [13] and Jiang [14] introduced a temperature-dependent channel-averaged transmittance of SEVIRI channel 4 $(\tau_4(\theta_v, T_{g,4}))$ defined by

$$\tau_4(\theta_v, T_{g,4}) = \frac{\int_0^\infty f_4(\lambda) R(\theta_v, T_{g,4}, \lambda) \tau(\theta_v, \lambda) d\lambda}{\int_0^\infty f_4(\lambda) R(\theta_v, T_{g,4}, \lambda) d\lambda}. \quad (13)$$

Consequently, the channel-averaged radiance in channel 4 $(L_4(\theta_v, T_4))$ can be rewritten as

$$L_4(\theta_v, T_4) = \tau_4(\theta_v, T_{g,4}) R_4(\theta_v, T_{g,4}) + L_{atm\uparrow 4}(\theta_v). \quad (14)$$

As shown in (14), to obtain $R_4(\theta_v, T_{g,4})$, the quantity $\tau_4(\theta_v, T_{g,4})$ is a key parameter that depends on the estimation of $T_{g,4}$. The change in $\tau_4(\theta_v, T_{g,4})$ was observed to be less than 0.6% when $T_{g,4}$ varies by 10 K [13], [14], which indicates that the quantity $\tau_4(\theta_v, T_{g,4})$ can be obtained with sufficient accuracy using an approximate temperature. Therefore, the quantity $R_4(\theta_v, T_{g,4})$ can be obtained as follows:

1) computation of the approximate brightness temperature $(T_{g,4a})$ in channel 4 at ground level using (4);
2) estimation of the average transmittance in SEVIRI channel 4 $(\tau_4(\theta_v, T_{g,4a}))$ using (13) with $T_{g,4a}$;
3) inversion of (14) to obtain $R_4(\theta_v, T_{g,4})$ with the estimated $\tau_4(\theta_v, T_{g,4a})$ in the second step.

Because the TIR channels (SEVIRI channels 9 and 10) are very sensitive to changes in the atmospheric WVC, a large error would be produced when using the time-nearest atmospheric data to obtain $R_j (j = 9$ and $10)$ for the images acquired at times other than the synoptic times (UTC: 05:57, 11:57, 17:57, and 23:57). Therefore, to address this limitation, a two-part semiempirical diurnal temperature cycle (DTC) model with six unknown parameters [25] is used for the temporal interpolation to obtain $T_{g,j} (j = 9$ and $10)$ at any times from those used at synoptic times. The DTC model is described by the following equations:

$$T_{g,j}^{day}(t) = a_j + b_j \cos(\beta_j(t - t_{d,j}))$$

$$\text{when } t \leq t_s \text{ for daytime} \quad (15)$$

$$T_{g,j}^{night}(t) = b_{1,j} + b_{2,j} \exp(\alpha_j(t - t_{s,j}))$$

$$\text{when } t > t_s \text{ for nighttime} \quad (16)$$

with

$$b_{2,j} = -\frac{b_j \beta_j \sin(\beta_j(t_{s,j} - t_{d,j}))}{\alpha_j}$$

$$b_{1,j} = a_j + b_j \cos(\beta_j(t_{s,j} - t_{d,j})) - b_{2,j}$$

where β_j is the angular frequency in channel $j (j = 9$ and $10)$, $t_{d,j}$ is the time when the $T_{g,j}$ reaches its maximum in channel j, $t_{s,j}$ is the starting time of attenuation in channel j, and α_j is the decay coefficient at nighttime in channel j.

Because atmospheric quantities are only available at four synoptic times in one day for each location, the DTC model is underdetermined with four measurements. To reduce the number of unknowns in the model and to make the model deterministic, $t_{d,j} (j = 9$ and $10)$ and $t_{s,j}$ in the model are taken as known parameters and are predetermined from the quantity T_j by assuming that the atmosphere between the ground and the satellite does not change $t_{d,j}$ and $t_{s,j}$ [26]. The DTC model described by (15) and (16) with predetermined $t_{d,j}$ and $t_{s,j}$ values is then fitted with a Levenberg–Marquardt least squares algorithm. However, at some locations, because of the constraint in the model related to sunrise time or cloud contaminations, only three $T_{g,j}$ values are available for fitting the DTC model, or only one $T_{g,j}$ value is eligible before $t_{s,j}$ even if four $T_{g,j}$ values are available. In this case, the parameter α_j in the DTC model is also assumed to be the same at the satellite and ground levels. Furthermore, due to the large fluctuation in temperature and the inaccuracy of the DTC model around sunrise, data from 2 h before sunrise to 2 h after sunrise are excluded to construct a more accurate TISI (and therefore to retrieve more accurate LSEs).

The procedures for performing atmospheric corrections of the TIR images are shown in Fig. 3. These procedures are primarily divided into three steps: 1) With the aid of MODTRAN 4.0, the atmospheric quantities at a spatial resolution of 0.25°/0.25° latitude/longitude at the synoptic times are estimated with the ECMWF profiles and other ancillary data required in MODTRAN, and the atmospheric effects for the SEVIRI images at each synoptic time are then corrected with spatial interpolated atmospheric quantities corresponding to SEVIRI pixels estimated with a bilinear interpolation method; 2) the parameters in the DTC model are derived from $T_j (j = 9$ and $10)$; and 3) the $T_{g,j} (j = 9$ and $10)$ at times other than the synoptic times is estimated from those at the synoptic times using the DTC model with predetermined $t_{d,j}, t_{s,j}$, or α_j.

Jiang et al. [13] and Jiang [14] assumed that the values of β_j and $t_{s,j} (j = 9$ and $10)$ in the DTC model derived from T_j were the same as those derived from $T_{g,j}$. To illustrate the improvement proposed in this study, two typical sites located at (33.225° N, 6.378° E) and (38.024° N, −3.834° E) are selected from the SEVIRI data from March 2, 2008 and March 13, 2009, respectively, and these data are atmospherically corrected using the DTC model with different known parameters. Fig. 4 shows the modeled $T_9, T_{g,9}$ at four synoptic times, the DTC simulated temperatures at ground level with known $t_{s,9}, t_{d,9}$, and α_9 (because only one $T_{g,9}$ at this site is eligible before $t_{s,9}$, the DTC at ground level is fitted with known values of $t_{s,9}, t_{d,9}$, and α_9), and that simulated with predetermined values of β_9 and
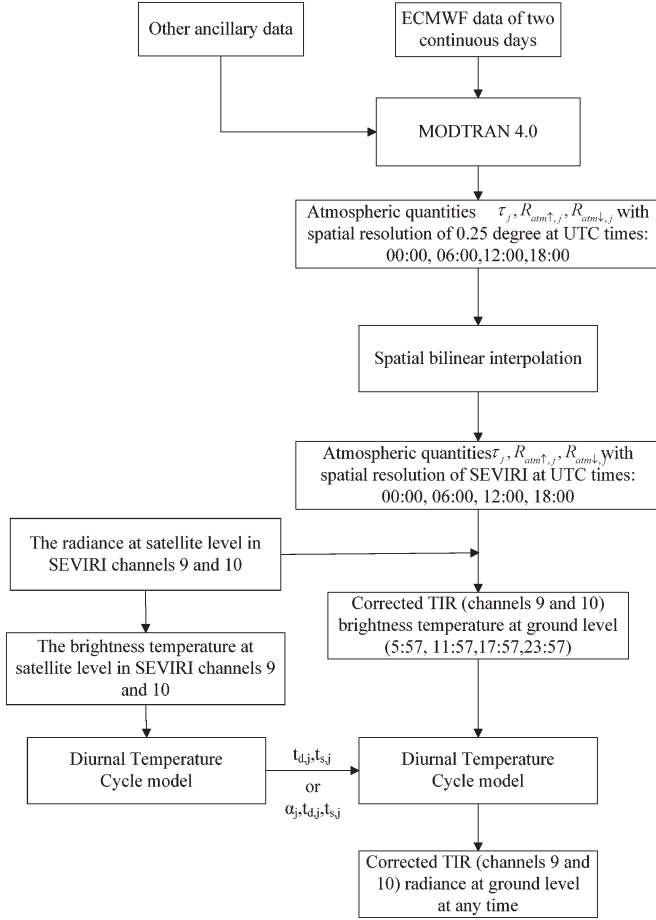
This article has been accepted for inclusion in a future issue of this journal. Content is final as presented, with the exception of pagination.

GAO *et al.*: IMPROVED ALGORITHM FOR RETRIEVING LSE AND LST FROM MSG-2/SEVIRI DATA 7

Fig. 3. Procedures for performing atmospheric corrections for the images of the TIR channels.

Fig. 4. Measured/modeled brightness temperatures at the satellite (T_9) and ground levels ($T_{g,9}$) in channel 9 with different known parameters (a) for the site located at 33.225° N, 6.378° E on March 2, 2008 and (b) for the site located at 38.024° N, −3.834° E on March 13, 2009.

$t_{s,9}$. It is noteworthy that, in Fig. 4, an unreasonable $t_{d,9}$ value (9.85 on March 2, 2008 and 9.73 on March 13, 2009) is derived when the DTC model at ground level is fitted with known β_9 and $t_{s,9}$ values, and the DTC fitted with the predetermined β_9 and $t_{s,9}$ values is obviously abnormal; the DTC fitted with known $t_{s,9}$, $t_{d,9}$, and α_9 values, on the other hand, is consistent with the actual situation. This result demonstrates that the assumption proposed in this study is more reasonable.

3) LSE Retrieval: To construct the TISI, the radiance $R_i(\theta v, Tg, i)(i = 4, 9, \text{and } 10)$ is calculated using the spatially interpolated atmospheric quantities estimated from the ECMWF data and then combined with the aforementioned DTC model. Using these $R_i(\theta v, Tg, i)$ values, the LSE can be retrieved with the following procedures:

1) The $E_{sun,4}$ value at any local time is predicted by assuming that $E_{sun,4}$ simply varies as a cosine function

$$E_{sun,4}(t) = A_s + B_s \cos \beta_s(t - 12) \tag{17}$$

where t is the local solar time and A_s, B_s, and β_s are unknown coefficients that can be predetermined using various $E_{sun,4}$ values. To accelerate the processing of ECMWF data, the $E_{sun,4}$ quantity is calculated every 2 h rather than every 15 min (the temporal resolution of the SEVIRI).
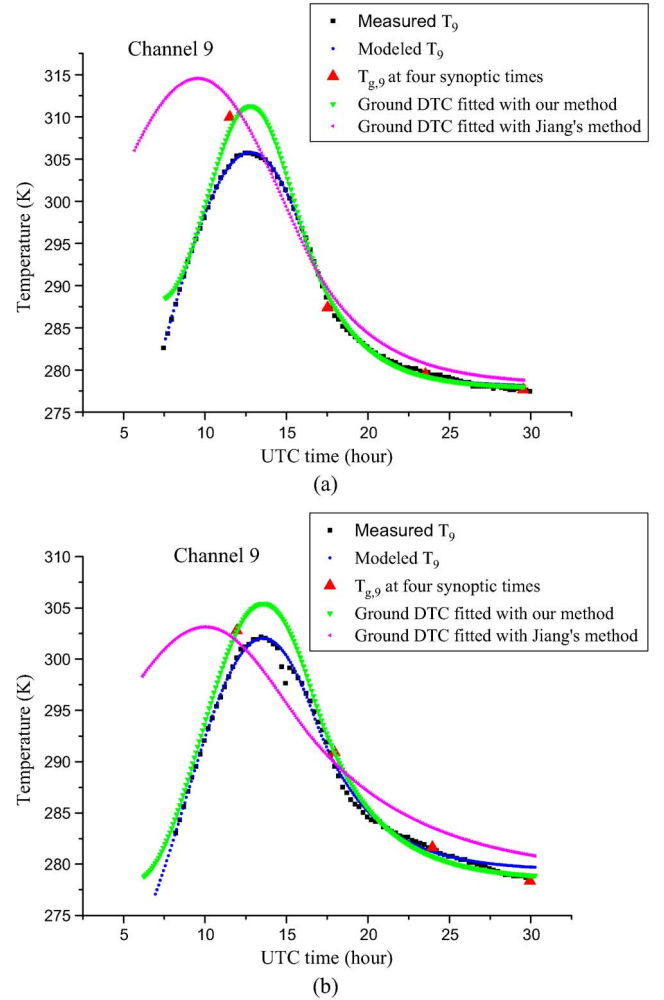
2) The values of $\rho_i(\theta_v, \theta_s, \varphi)$ in channel 4 ($\rho_4(\theta_v, \theta_s, \varphi)$) with different solar illumination directions are calculated assuming $C^{day}/C^{night} = 1.0$ in (7), which is a rather good approximation of the $\rho_4(\theta_v, \theta_s, \varphi)$ estimation [13], [14]. In this procedure, all of the daytime data are used, and data at 23:57 UTC are selected because of the following: 1) The TISI at night is stable (constant value during the nighttime); 2) ECMWF profile data are only available at 00:00, 06:00, 12:00, and 18:00 UTC every day, and therefore, the SEVIRI data acquired at 23:57 UTC can be atmospherically corrected using ECMWF atmospheric profiles; and 3) for the studied region, all of the pixels observed at 23:57 UTC are measured during the night when no direct or diffuse solar radiation is present.

3) Based on the RossThick–LiSparse-R model and Kirchhoff's law, $\varepsilon_4(\theta_v)$ is derived using (8) and (9). A Levenberg–Marquardt minimization scheme is utilized to determine the parameters $K_{4,iso}$, $K_{4,vol}$, and $K_{4,geo}$ in (9) for each pixel using various values of $\rho_4(\theta_v, \theta_s, \varphi)$ with different solar illumination directions. In the fitting procedure, if the absolute difference between the

This article has been accepted for inclusion in a future issue of this journal. Content is final as presented, with the exception of pagination.

8   IEEE TRANSACTIONS ON GEOSCIENCE AND REMOTE SENSING

measured and modeled bidirectional reflectivity is two times greater than the root-mean-square error (RMSE), this measurement is eliminated in the next fitting procedure until the number of measurements is reduced by 30%; in this manner, the bidirectional reflectivity model is not sensitive to the errors in the reflectivities, and the parameters $K_{4,iso}$, $K_{4,vol}$, and $K_{4,geo}$ can be correctly inverted. However, in Jiang's work [14], the minimum number of measurements was set to 7, which may result in local optimal solutions rather than global optimal solutions.

4) Due to the stability of the TISI at night and the availability of ECMWF data, the nighttime $TISI_{4,9}$ and $TISI_{4,10}$ at 23:57 UTC are calculated and used to estimate $\varepsilon_9(\theta_v)$ and $\varepsilon_{10}(\theta_v)$ according to (12). However, Jiang *et al.* [13] and Jiang [14] derived $\varepsilon_{10}(\theta_v)$ from $\varepsilon_9(\theta_v)$ using $TISI_{9,10}$. This derivation resulted in the propagation of error in $\varepsilon_9(\theta_v)$ to $\varepsilon_{10}(\theta_v)$.

C. LST Retrieval Method

It is worth noting that the estimated errors in LSE in SEVIRI channels 9 and 10 with the TISI method are not independent; in particular, the error in the emissivity difference between the two adjacent channels ($\Delta\varepsilon$) is very small. Because the LST retrieval using the single-channel method is sensitive to the error of atmospheric corrections but the LSE retrieval using the TISI method is not and given that the error in $\Delta\varepsilon$ is small, the SW method can be used to derive the LST with an acceptable accuracy [17]. In this paper, a generalized SW method (GSW) proposed by Becker and Li [15] and developed by Wan and Dozier [8] is used, in which the LST is retrieved from the MSG-2/SEVIRI data in the form of

$$T_s = A_0 + \left(A_1 + A_2 \times \frac{1-\varepsilon}{\varepsilon} + A_3 \times \frac{\Delta\varepsilon}{\varepsilon^2}\right) \times \frac{T_9 + T_{10}}{2}$$

$$+ \left(B_1 + B_2 \times \frac{1-\varepsilon}{\varepsilon} + B_3 \times \frac{\Delta\varepsilon}{\varepsilon^2}\right) \times \frac{T_9 - T_{10}}{2} \quad (18)$$

where ε is the averaged emissivity [$\varepsilon = (\varepsilon_9 + \varepsilon_{10})/2$], $\Delta\varepsilon = (\varepsilon_9 - \varepsilon_{10})$, and A_0, A_1, A_2, A_3, B_1, B_2, and B_3 are unknown coefficients for a given VZA and a given subrange of ε, LST, and WVC which must be predetermined.

The coefficients A_i, B_i and $A_0(i = 1, 2, 3)$ in (18) can be predetermined either from the ground LST measured synchronously with satellite brightness temperatures (T_j, $j = 9, 10$) or from simulated data under various atmospheric and surface conditions by statistical regression. To render the algorithm operational, the determination of the GSW coefficients A_i, $B_i(i = 1, 2, 3)$, and A_0 is performed using numerical simulations, as insufficient high quality simultaneous *in situ* measurements of the LST for a wide range of surface types and atmospheric conditions are available to permit a good determination of the coefficients.

In the simulations using MODTRAN 4.0 [27] to acquire the values of coefficients A_i, $B_i(i = 1, 2, 3)$, and A_0 in (18), 1413 clear-sky atmosphere profiles are used in combination

with various land surface conditions (LSE and LST), VZA, and spectral response functions of SEVIRI channels 9 and 10 to drive MODTRAN to simulate $T_j(j = 9$ and $10)$ [28], [29]. For each VZA (11 VZAs at the surface (0°, 10.16°, 20.33°, 30.52°, 35.63°, 40.76°, 45.91°, 51.08°, 56.31°, 61.6°, and 67°) are considered in this paper), various values of $T_j(j = 9$ or $10)$ with different atmospheric profiles and surface conditions are simulated according to (4). Furthermore, to improve the accuracy of LST retrieval for each VZA, the WVC, LSE, and LST are divided into several tractable subranges, i.e., WVC: 0–1.5, 1.0–2.5, 2.0–3.5, 3.0–4.5, 4.0–5.5, and 5.0–6.5 g/cm²; ε: 0.90–0.96 and 0.94–1.0; and LST: $\leq$280.0 K, 275–295 K, 290–310 K, 305–325 K, and $\geq$320 K. The coefficients A_0, A_1, A_2, A_3, B_1, B_2, and B_3 in (18) for each subrange of ε, LST and WVC can be determined using the minimization procedure with the simulated data. The results indicate that the RMSE of the retrieved LST varies with the VZA and the atmospheric WVC and that the RMSEs are within 1.0 K for all subranges where the VZA $< 30°$ and WVC < 4.25 g/cm².

Furthermore, because the atmospheric WVC is used to select the optimal coefficients A_i, $B_i(i = 1, 2, 3)$, and A_0 in the GSW method, an accurate WVC is not required, provided that the estimated WVC is within the same range as the actual WVC. The method proposed by Li *et al.* [30] is used to estimate the WVC at the spatial resolution of several pixels from the SEVIRI measurements of channels 9 and 10. If this method fails (if the square of the correlation coefficient is less than 0.95), the WVCs provided by the ECMWF data are used to obtain the WVC corresponding to the relevant pixel with a temporal and spatial linear interpolation.

In practice, the LST is estimated in two steps. First, the approximate LST is estimated with the coefficients for the entire LST; then, a more accurate LST is determined using the coefficients for the LST subrange containing the approximate LST [31].

Fig. 5 shows the key procedures for retrieving the LSE and LST from SEVIRI data. These procedures are composed of four parts: 1) Data preparation: The MSG-2/SEVIRI radiances, corresponding cloud masks, land/water masks, ECMWF profiles, and other ancillary data sets, such as view geometry data and geolocation information (latitudes and longitudes) are extracted or preprocessed using SPT software and self-developed C++ programs; 2) atmospheric correction: with the aid of MODTRAN 4.0, the atmospheric effects for the SEVIRI channels 4, 9, and 10 are corrected. For channels 9 and 10, the DTC at ground level has the same parameters [$t_{d,j}$ and $t_{s,j}$ or α_j, $t_{d,j}$, and $t_{s,j}(j = 9$ and $10)$] as the DTC at the satellite level rather than β_j and $t_{s,j}$; 3) LSE retrieval: LSEs in channels 4, 9, and 10 are derived based on the TISI concept and the bidirectional reflectivity model (RossThick–LiSpare-R model), and in the LSE retrieval, the schemes used to fit the bidirectional reflectivity model and retrieve the LSE in the SEVIRI channel 10 are improved; and 4) LST retrieval: the LST is estimated using the GSW [see (18)] with the knowledge of $T_j(j = 9$ and $10)$, the predetermined coefficients [A_i, $B_i(i = 1, 2, 3)$ and A_0] in (18), $\varepsilon_j(\theta_v)(j = 9$ and $10)$, and the WVC either estimated with the method proposed by Li *et al.* [30] or provided by the ECMWF data.

This article has been accepted for inclusion in a future issue of this journal. Content is final as presented, with the exception of pagination.

GAO *et al.*: IMPROVED ALGORITHM FOR RETRIEVING LSE AND LST FROM MSG-2/SEVIRI DATA   9
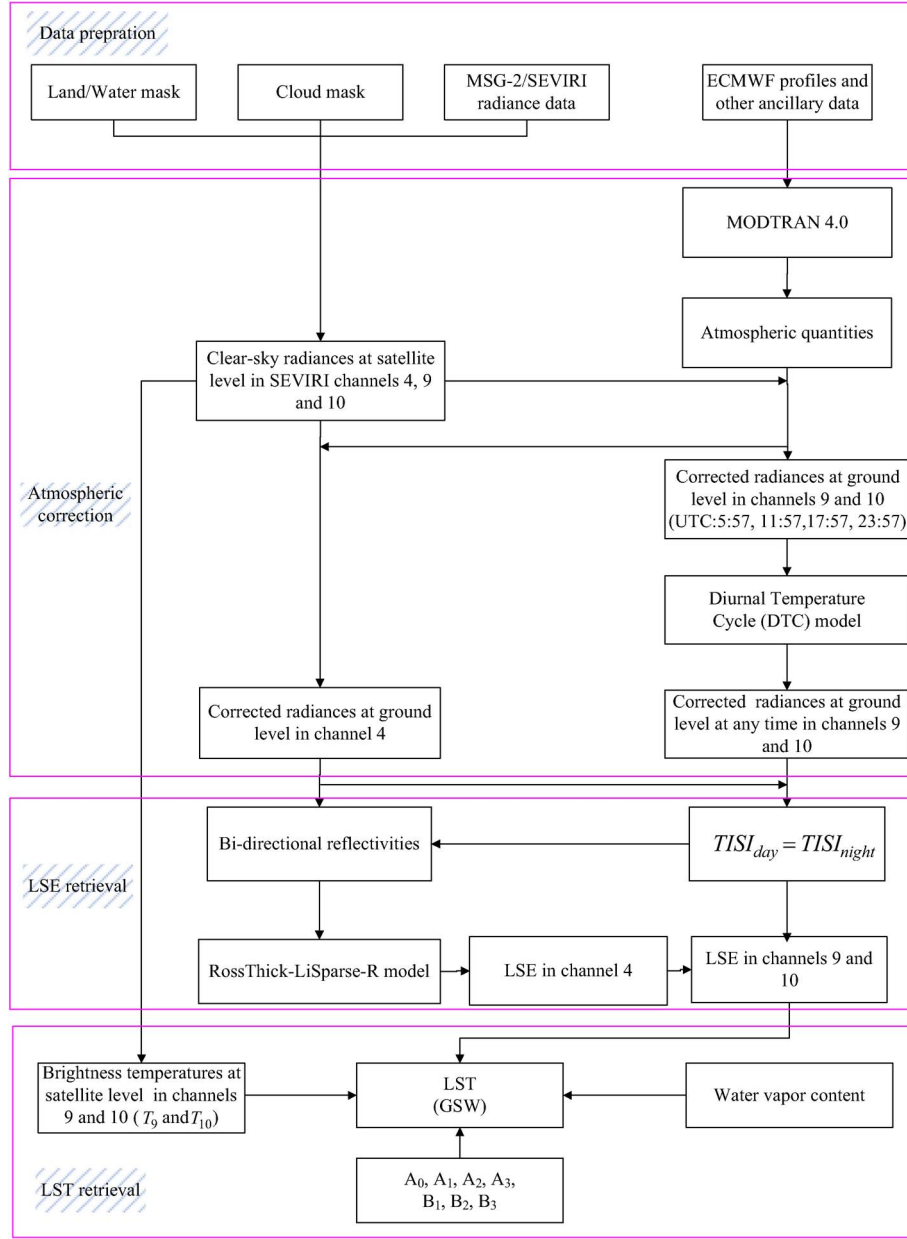

Fig. 5.   Procedures for retrieving the LSE/LST from the MSG-2/SEVIRI data.

IV. RESULTS AND CROSS-VALIDATION

A. Results

To analyze the performance of the algorithm described in Section III under different climatic and atmospheric conditions, the algorithm is applied to these data sets on four clear-sky days (August 22, 2009, March 13, 2009, July 3, 2008, and March 2, 2008) after data processing of the MSG Level 1.5 product, the cloud filtering steps, and the atmospheric correction with ECMWF data and other ancillary data sets (DEM data, geolocation data (longitude and latitude), SEVIRI view geometry data, etc.). As an example, Fig. 6 shows the spatial variation of the derived LSE in channels 4, 9, and 10 [see Fig. 6(a)–(c), respectively] and the LST at 11:12 (UTC time) [see Fig. 6(d)] derived from SEVIRI data over the entire study area on August 22, 2009. As shown in this figure, the entire image is spatially heterogeneous, and the LSEs over the vegetated surfaces are

usually higher than those over bare surfaces. The southern region of the Maghreb, which is dominated by bare soils, presents considerably higher LSTs than the other regions. However, because of the cloud contamination and limitations of the algorithm (such as the requirements for a minimum number of observations in the DTC model and the bidirectional reflectivity model), a number of LSEs/LSTs are not successfully derived. This phenomenon also occurs on the other days.

As mentioned in Section III, some improvements are adopted for the retrievals of the LSE/LST from the MSG-2/SEVIRI data. The effects of these improvements on results are analyzed with the data sets on the aforementioned four clear-sky days in terms of the following three aspects.

1) The DTC at ground level has the same parameters [$t_{d,j}$ and $t_{s,j}$ or α_j, $t_{d,j}$, and $t_{s,j}(j = 9$ and 10)] as the DTC at the satellite level rather than β_j and $t_{s,j}$. As illustrated in

This article has been accepted for inclusion in a future issue of this journal. Content is final as presented, with the exception of pagination.

10

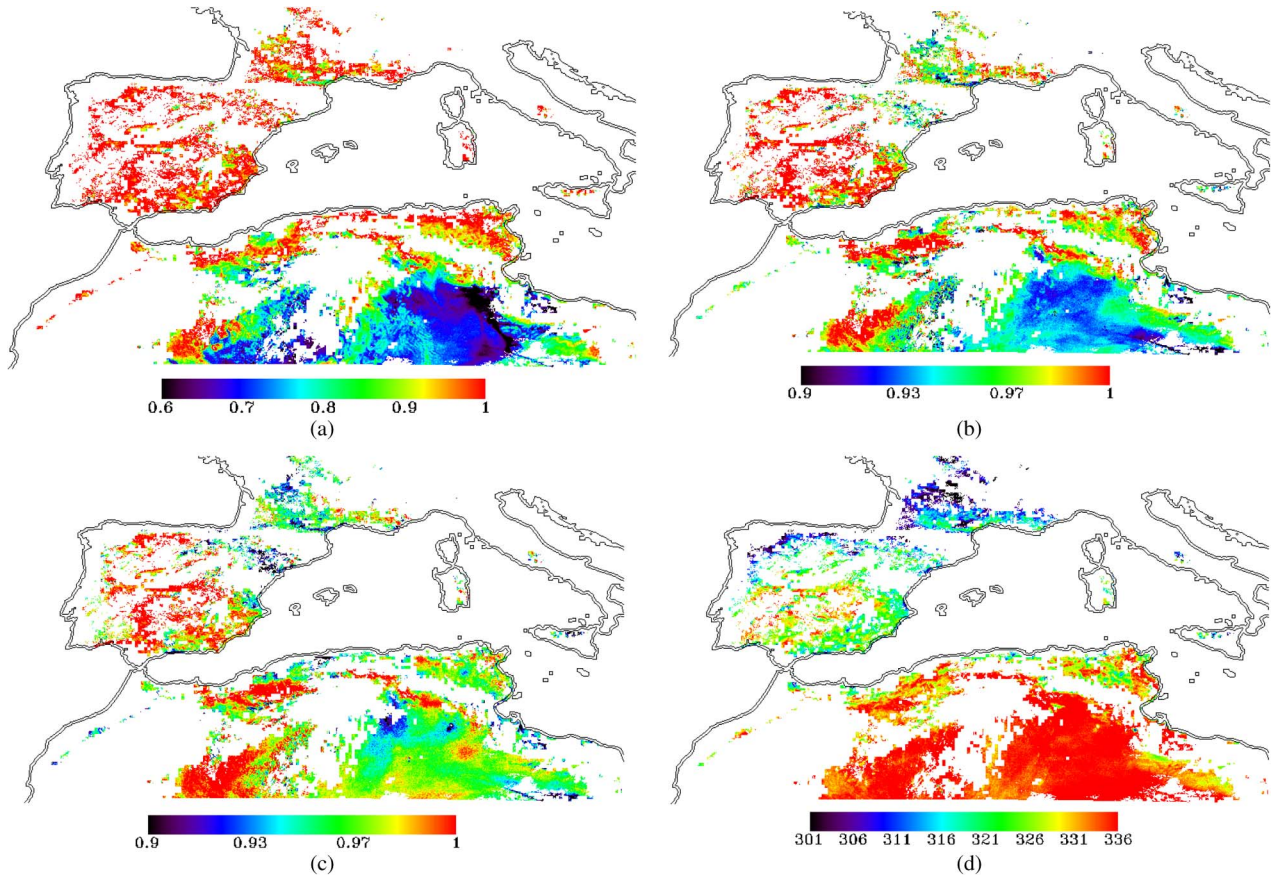IEEE TRANSACTIONS ON GEOSCIENCE AND REMOTE SENSING

Fig. 6. Maps of the LSEs in SEVIRI channels 4, 9, and 10 and the LSTs at 11:12 (UTC time) retrieved from the SEVIRI data on August 22, 2009. (a) LSE in channel 4. (b) LSE in channel 9. (c) LSE in channel 10. (d) LSTs at 11:12.
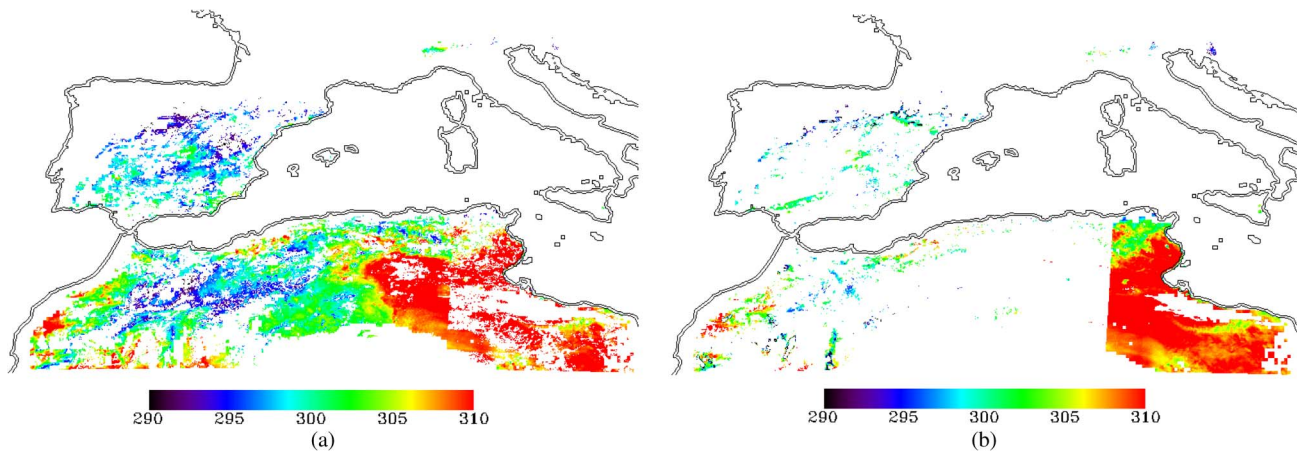

Fig. 7. Maps of the brightness temperature for surface-leaving radiances in channel 9 at 11:12, March 2, 2008 (UTC time). (a) Based on the schemes proposed in this paper. (b) Based on the schemes proposed by Jiang *et al.* [13] and Jiang [14].

Fig. 4, unreasonable DTC coefficients are usually derived with predetermined β_j and $t_{s,j}$ values when only one $T_{g,j}$ value is eligible before $t_{s,j}$, even if four $T_{g,j}$ values are available, which results in the failure of the atmospheric correction with the DTC model for the TIR data. This improvement can be typically illustrated by the $T_{g,9}$ obtained on March 2, 2008 and March 13, 2009, as the number of $T_{g,9}$ values significantly increases (see Figs. 7

and 8) from 28 945 to 58 956 on March 2, 2008 and from 32 512 to 37 642 on March 13, 2009 after improvements on the algorithm are made. For the data in channel 9 on August 22, 2009 and July 3, 2008, the differences between the value $T_{g,9}$ at 11:12 (UTC time) based on the schemes proposed in this study (denoted as LSBT1) and the value $T_{g,9}$ at 11:12 derived using the original schemes presented by Jiang *et al.* [13] and Jiang [14] (denoted

This article has been accepted for inclusion in a future issue of this journal. Content is final as presented, with the exception of pagination.

GAO *et al.*: IMPROVED ALGORITHM FOR RETRIEVING LSE AND LST FROM MSG-2/SEVIRI DATA
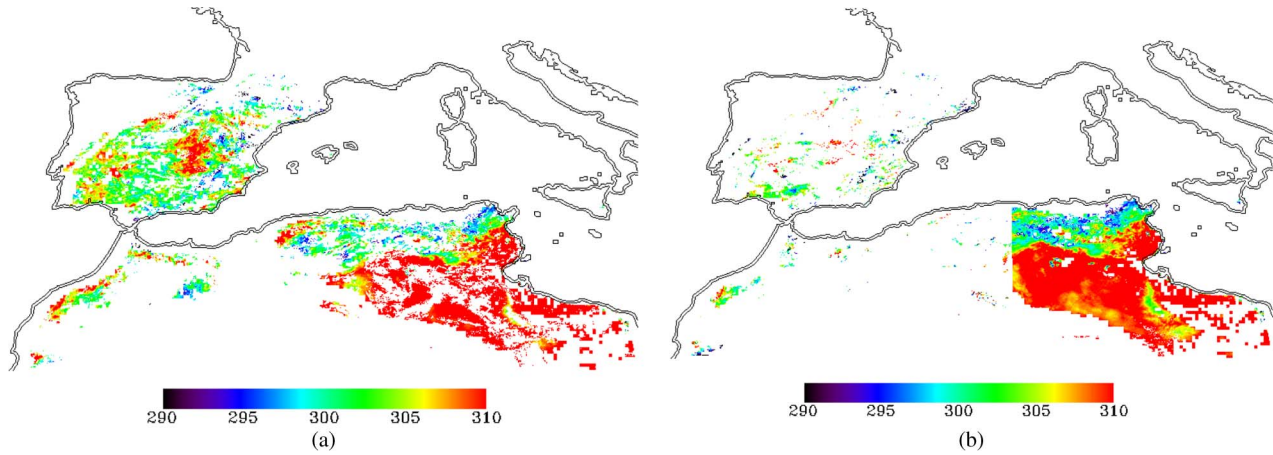
11

Fig. 8.   Maps of the brightness temperature for surface-leaving radiances in channel 9 at 11:12, March 13, 2009 (UTC time). (a) Based on the schemes proposed in this paper. (b) Based on the schemes proposed by Jiang *et al.* [13] and Jiang [14].
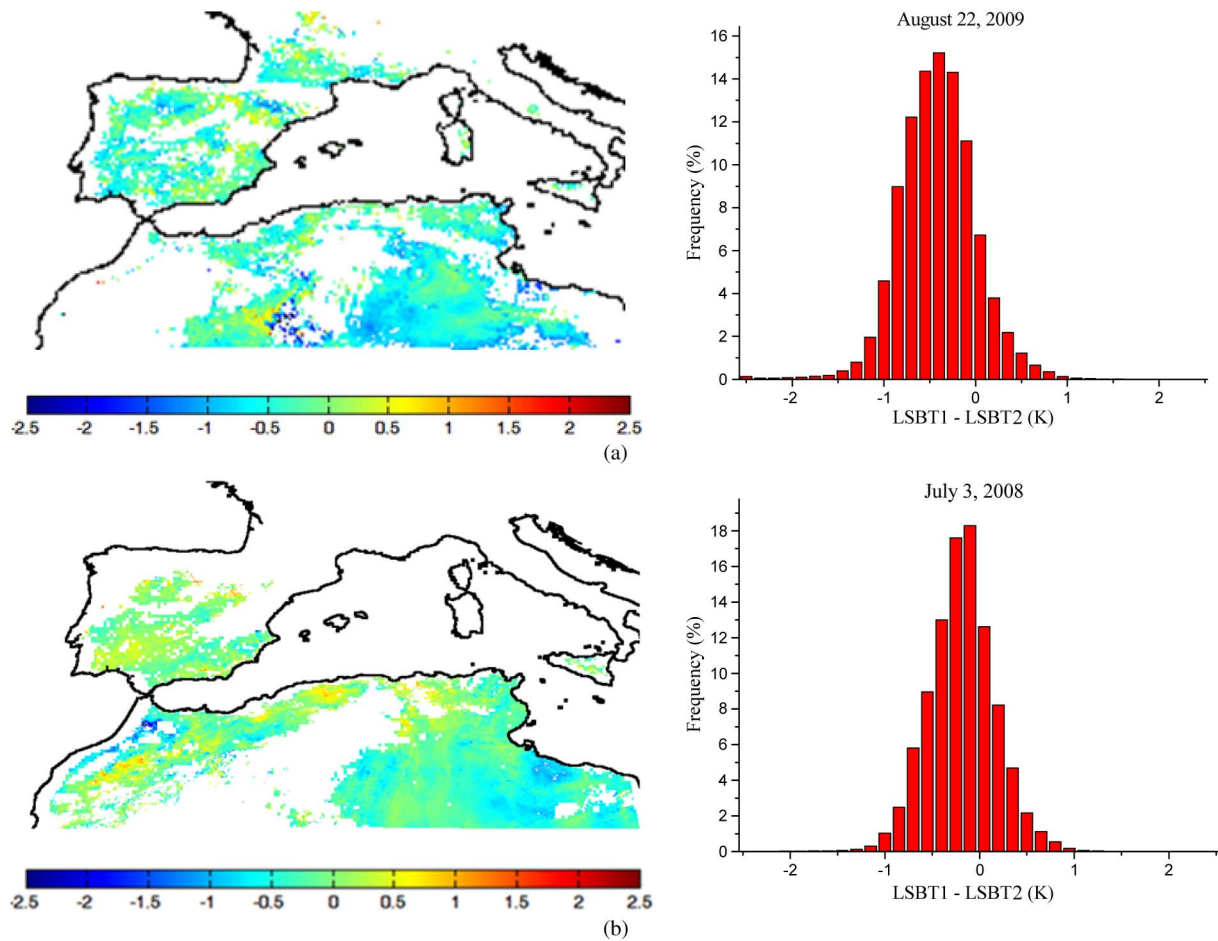

Fig. 9.   Maps of the differences between the LSBT1 and LSBT2 in channel 9 at 11:12 (a) on August 22, 2009 and (b) on July 3, 2008 (UTC time) and the corresponding histograms of these differences. LSBT1 and LSBT2 are the brightness temperatures for surface-leaving radiances based on the schemes proposed in this study and those derived using the original schemes proposed by Jiang *et al.* [13] and Jiang [14], respectively.

as LSBT2) and the corresponding histograms of these differences are shown in Fig. 9. It is worth noting that the value of LSBT1 is lower than the value of LSBT2 in most cases, and the differences between LSBT1 and LSBT2 are within 1 K. Similar results are obtained for March 13, 2009 and March 2, 2008.

2) In step 3 of retrieving the LSE, if the absolute difference between the measured and the modeled bidirectional reflectivity is two times greater than the RMSE, the measurement is discarded until the number of measurements (minimum number) is reduced by 30% (denoted as Scheme 1) rather than setting the minimum number of

This article has been accepted for inclusion in a future issue of this journal. Content is final as presented, with the exception of pagination.

12

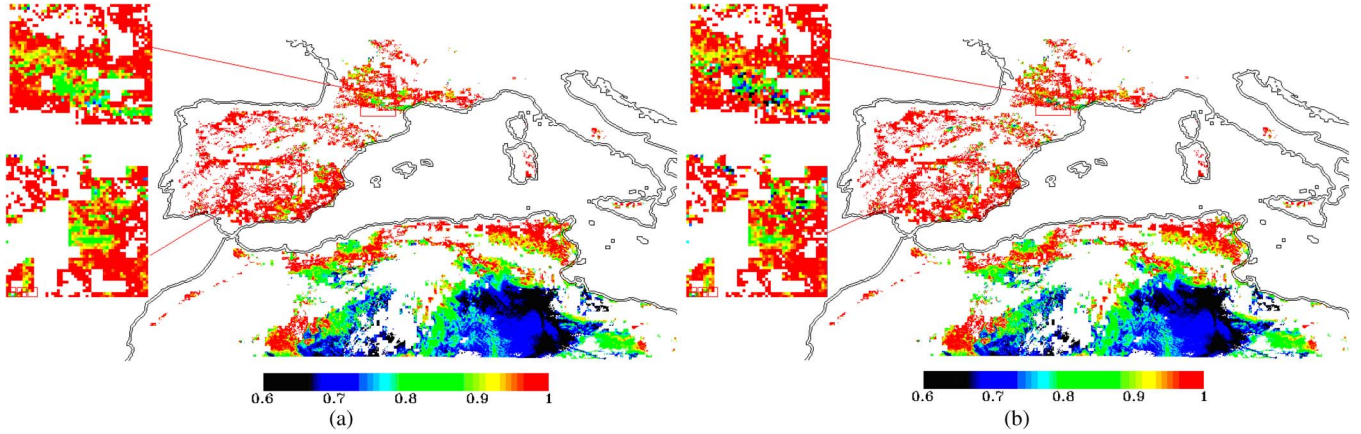IEEE TRANSACTIONS ON GEOSCIENCE AND REMOTE SENSING

Fig. 10. Maps of the LSEs in channel 4 retrieved with the reflectivities on August 22, 2009 using different schemes. (a) Using the schemes proposed in this study. (b) Using the schemes proposed by Jiang *et al.* [13] and Jiang [14].
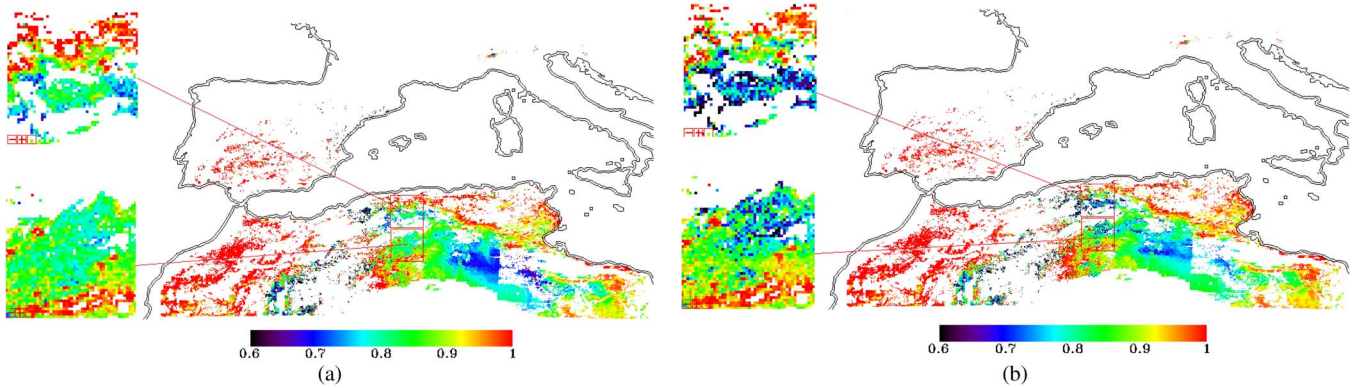

Fig. 11. Maps of the LSEs in channel 4 retrieved with the reflectivities on March 13, 2009 using different schemes. (a) Using the schemes proposed in this study. (b) Using the schemes proposed by Jiang *et al.* [13] and Jiang [14].

measurements to 7 (denoted as Scheme 2), which ensures that the bidirectional reflectivity model is not sensitive to the errors in the reflectivities and more reasonable values of $\varepsilon_4(\theta_v)$ are obtained. To illustrate this improvement, we retrieve the $\varepsilon_4(\theta_v)$ using the same values of $\rho_4(\theta_v, \theta_s, \varphi)$ using Schemes 1 and 2, respectively; the results of this analysis on August 22 and March 13, 2009 are shown in Figs. 10 and 11, respectively. It is obvious that there are less abnormal LSEs (black pixels) [see Figs. 10(a) and 11(a)] over the two small areas (red boxes) after improvement.

3) The $\varepsilon_{10}(\theta_v)$ value is derived from $\varepsilon_4(\theta_v)$ rather than from $\varepsilon_9(\theta_v)$. The differences between the $\varepsilon_{10}(\theta_v)$ value retrieved from $\varepsilon_4(\theta_v)$ (denoted as LSE10$_1$) and the $\varepsilon_{10}(\theta_v)$ value derived from $\varepsilon_9(\theta_v)$ (denoted as LSE10$_2$) are calculated; most of the differences between LSE10$_1$ and LSE10$_2$ on the four days are within 0.005. As an example, the corresponding histograms of these differences on August 22, 2009 and July 3, 2008 are shown in Fig. 12.

As presented earlier, the improved algorithm is more effective and reasonable. To quantify the differences between the SEVIRI-derived LSE/LST (denoted as SEVIRI LSE1/LST1) retrieved with the improved algorithms and the SEVIRI-derived LSE/LST (denoted as SEVIRI LSE2/LST2) retrieved based on the original schemes proposed by Jiang *et al.* [13] and Jiang [14], the differences between the SEVIRI LSE1 and the SEVIRI LSE2 in channels 4, 9, 10 and the differences between the SEVIRI LST1 and SEVIRI LST2 at 11:12 (UTC time) are calculated. On the previously mentioned four days (August 22, 2009, March 13, 2009, July 3, 2008, and March 2, 2008), the LSE differences are within 0.1 for the most cases in channel 4 and within 0.05 in channels 9 and 10; the LST differences are within 2 K in most cases. As an example, the LSE/LST differences on August 22, 2009 and the corresponding histograms of these differences are displayed in Fig. 13. It is worth noting that the LSE differences in channel 4 are considerably higher than those in channels 9 and 10; more than 85% of the LSE differences are within 0.05 for channel 4 and 0.02 for channels 9 and 10, and more than 85% of the LST differences are within 1.0 K, although in some instances, differences greater than 2.0 K are also observed. Moreover, the diurnal cycles of SEVIRI LST1/LST2 on August 22, 2009 and their differences in two homogeneous areas (geographic coordinates: 35.176° N, 5.001° W and 34.493° N, 2.527° W) covered by trees and shrubs, respectively, are displayed in Fig. 14. It is worth noting that the differences between SEVIRI LST1 and SEVIRI LST2 over the tree-covered area are within 0.65 K, while the differences over the shrub-covered area range from −1.0 K to −1.5 K.
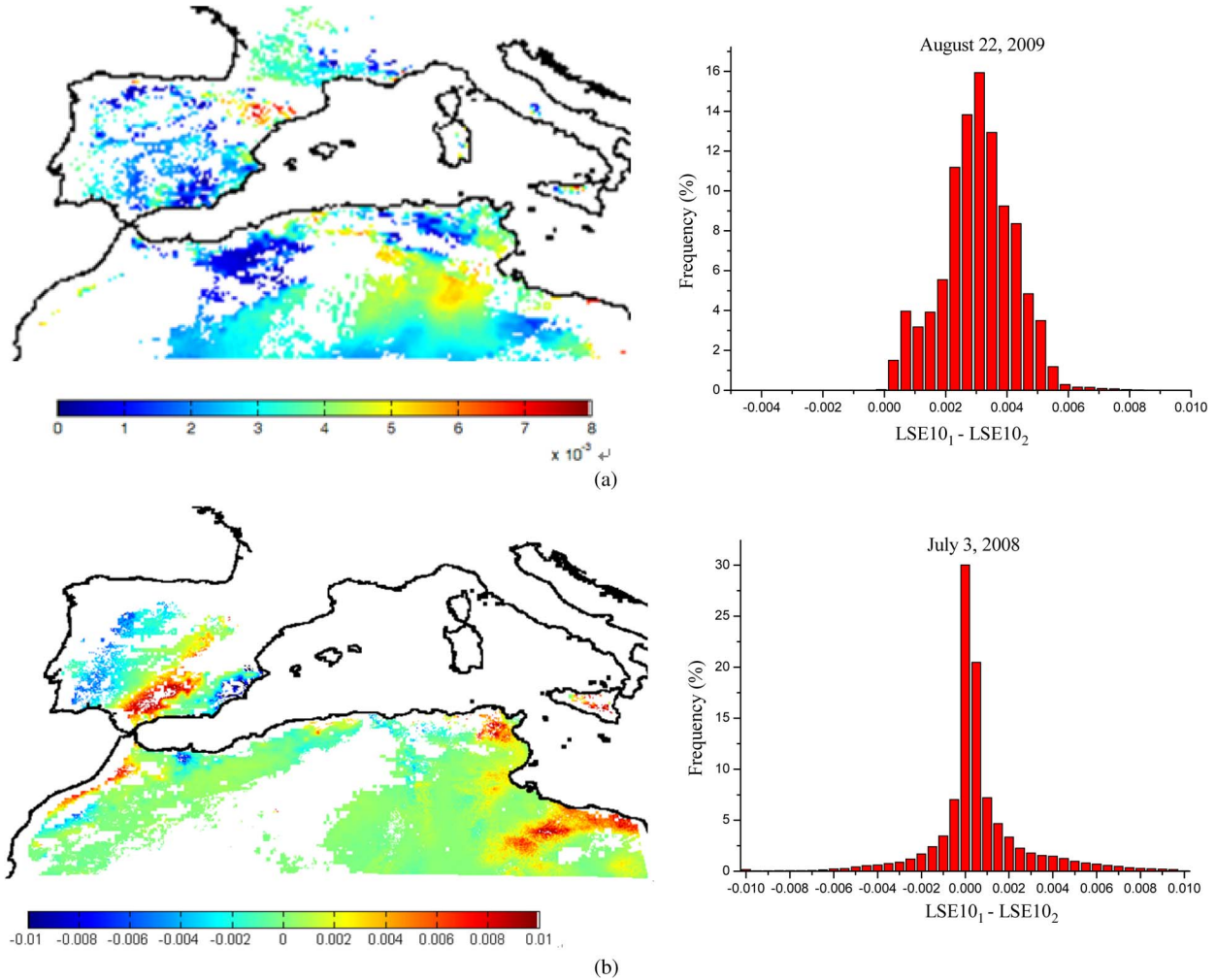
This article has been accepted for inclusion in a future issue of this journal. Content is final as presented, with the exception of pagination.

GAO *et al.*: IMPROVED ALGORITHM FOR RETRIEVING LSE AND LST FROM MSG-2/SEVIRI DATA   13

(a)

(b)

Fig. 12.   Maps of the differences between the $LSE10_1$ and $LSE10_2$ (a) on August 22, 2009 and (b) on July 3, 2008 and the corresponding histograms of the differences. $LSE10_1$ and $LSE10_2$ are the LSEs in channel 10 derived from the LSEs in channels 4 and 9, respectively.

B. Preliminary Cross-Validation

After data preprocessing, the qualified SEVIRI LST1 is cross-validated with the MODIS LST over the entire study area on the two clear-sky days (August 22, 2009 and July 3, 2008). The LST differences between the SEVIRI LST1 and the MODIS LST as a function of the MODIS LST and the histograms of the LST differences are shown in Fig. 15. It is noteworthy that the differences between the SEVIRI LST1 and the MODIS LST have no obvious relationship with the MODIS LST; approximately more than 70% of the LST differences are within 2.5 K on both August 22, 2009 and July 3, 2008, and the differences in LST tend to be lower at night than during the day, which may be explained by the relatively homogeneous thermal conditions of the Earth's surface at night. However, in several instances, the differences between the SEVIRI LST1 and the MODIS LST on August 22, 2009 reach approximately 10 K, which may have been caused by the misdetection of clouds.

V. CONCLUSION

Because the LST and LSE are key characteristics of the land surface, the retrieval of their values from space has been studied

for several decades. Based on the studies of Jiang *et al.* [13] and Jiang [14], an improved operational algorithm is developed in this paper to determine both the LSE and LST from MSG-2/SEVIRI measurements. Three components of the day/night TISI-based algorithm for retrieving the LSE from SEVIRI data are improved: the atmospheric correction, the fitting of the bidirectional reflectivity model, and the retrieval of the LSE in SEVIRI channel 10. The GSW method proposed by Becker and Li [15] and improved by Wan and Dozier [8] is then used to retrieve the LST with the knowledge of the retrieved LSE and the coefficients in (18) $[A_i, B_i (i = 1, 2, 3)$, and $A_0]$ that were predetermined during a numerical simulation under various atmospheric and surface conditions with the TIGR 2000 data set.

Applying our improved algorithm to the SEVIRI data under different climatic and atmospheric conditions reveals that the improved atmospheric correction algorithm resolves the problem that prevented the original algorithm proposed by Jiang *et al.* [13] and Jiang [14] from being applied to specific issues successfully, particularly for the atmospheric correction in regions with a late local sunrise time; less abnormal LSEs are obtained with the improved algorithm, illustrating that the improved algorithm is more reasonable and efficient.
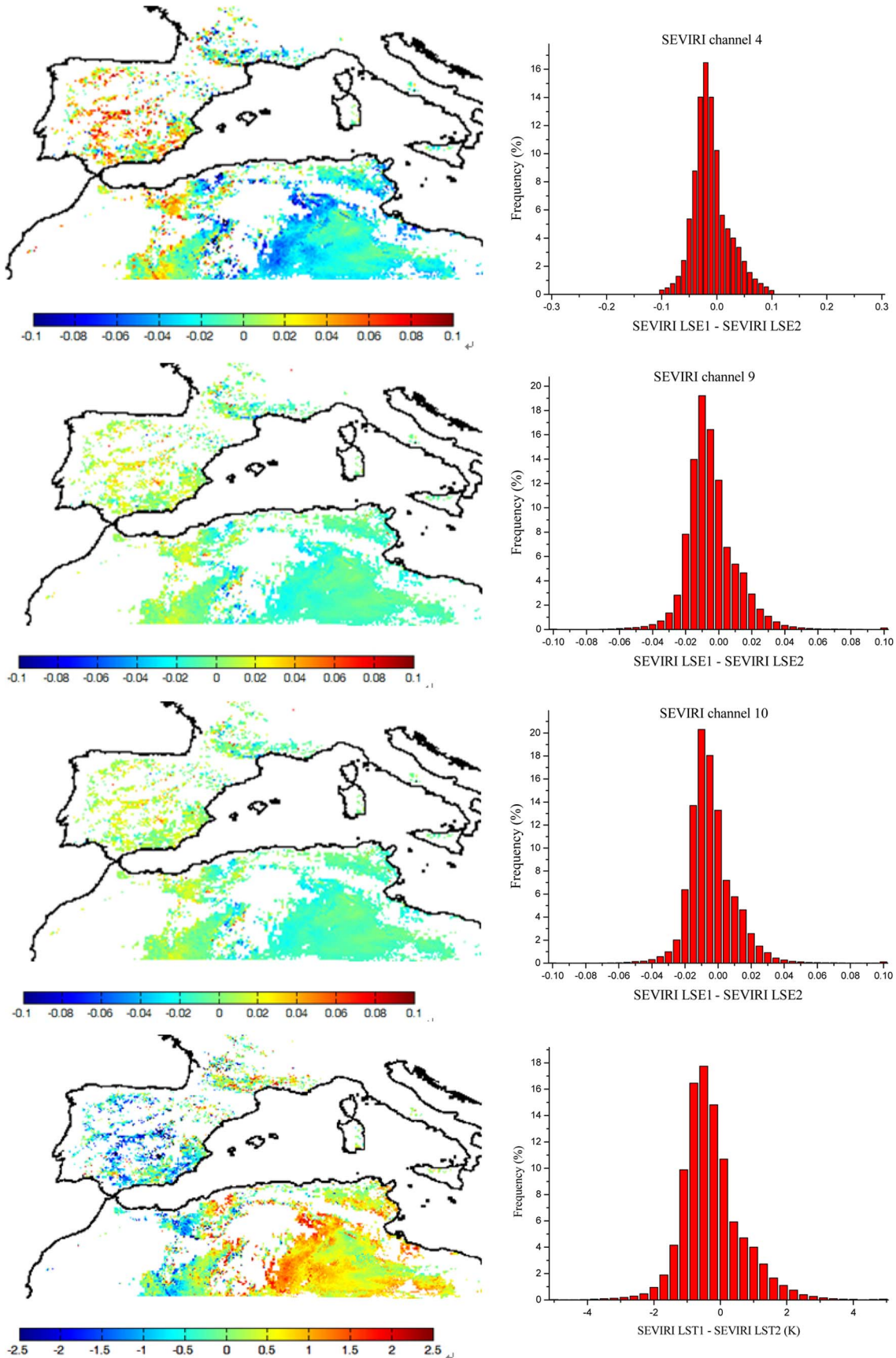
Fig. 13. Histograms of the differences between the SEVIRI LSE1 and the SEVIRI LSE2 on August 22, 2009 and the corresponding differences between the SEVIRI LST1 and the SEVIRI LST2 at 11:12 (UTC time). SEVIRI LSE1/LST1 is the LSE/LST retrieved using the algorithms proposed in this study, and SEVIRI LSE2/LST2 is the LSE/LST retrieved based on the original schemes proposed by Jiang *et al.* [13] and Jiang [14].

This article has been accepted for inclusion in a future issue of this journal. Content is final as presented, with the exception of pagination.

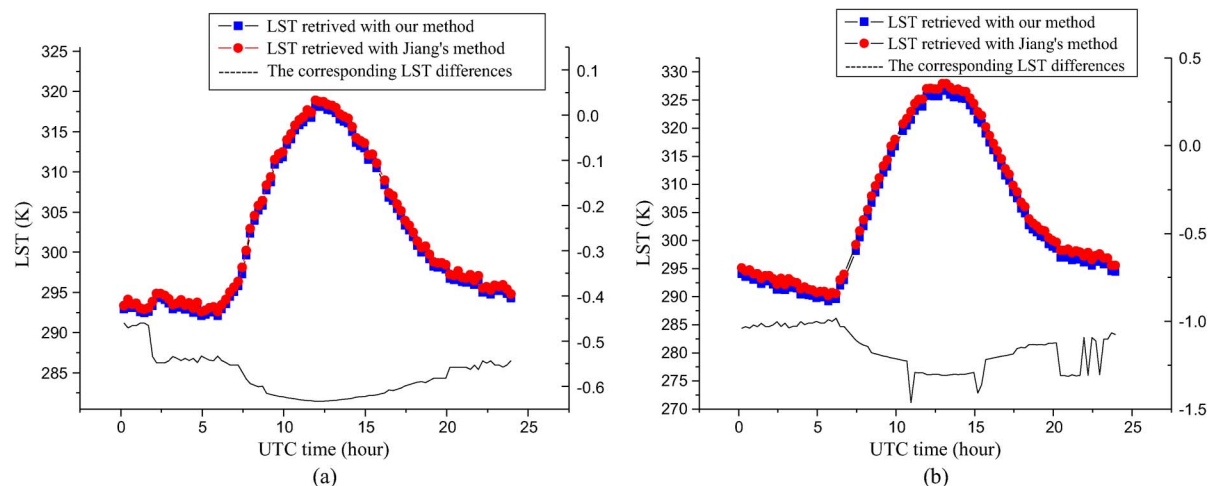GAO *et al.*: IMPROVED ALGORITHM FOR RETRIEVING LSE AND LST FROM MSG-2/SEVIRI DATA 15

Fig. 14. Diurnal cycles of LST on August 22, 2009, retrieved with our method and Jiang's method, at two respective sites. (a) 35.176° N, 5.001° W, covered by trees. (b) 34.493° N, 2.527° W, covered by shrubs.
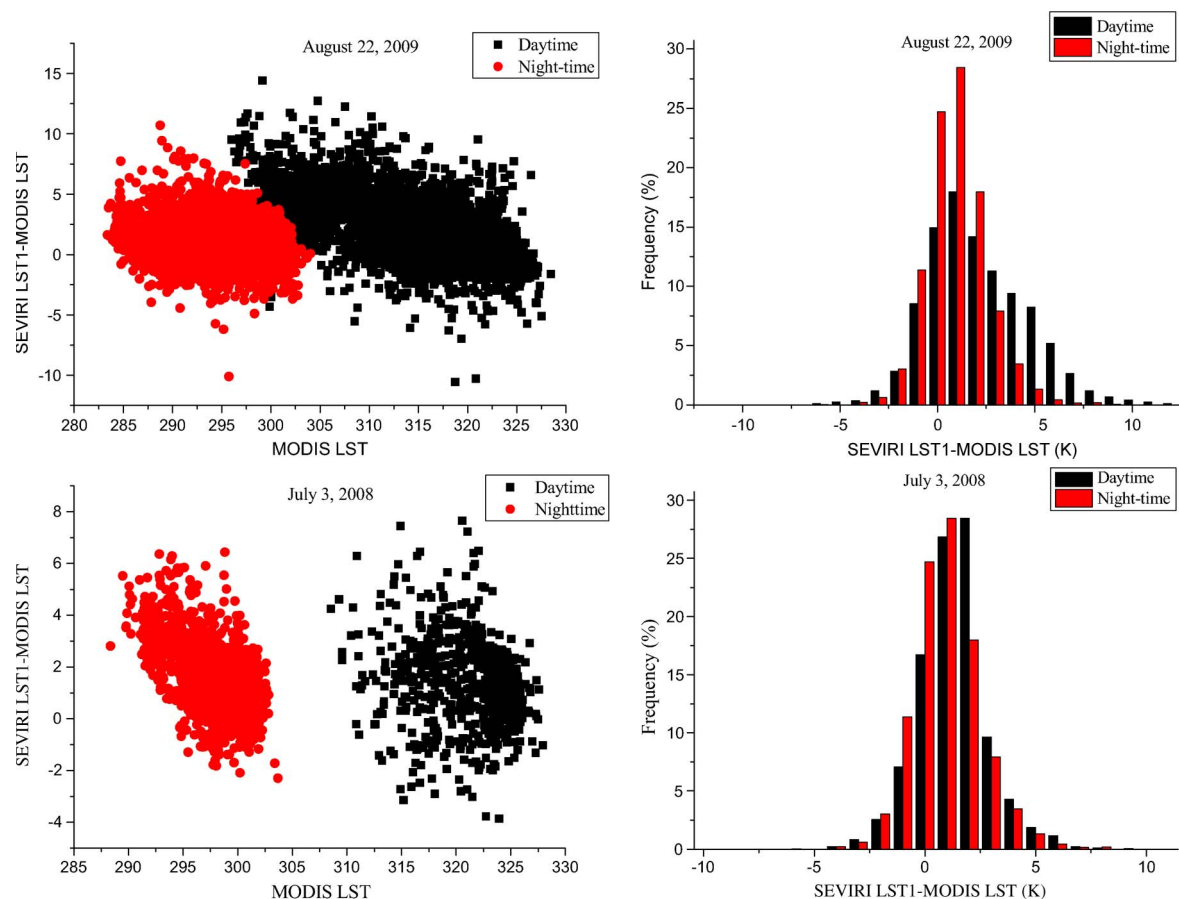

Fig. 15. Differences between the SEVIRI LST1 and the MODIS LST as a function of the MODIS LST and the corresponding histograms of their LST differences on August 22, 2009 and July 3, 2008. The SEVIRI LST1 is the LST retrieved in this study, and the MODIS LST is the LST extracted from the V5 MOD11B1 product.

To preliminarily validate the LST data (SEVIRI LST1) derived from the SEVIRI measurements obtained using the improved algorithm, cross-validations are conducted on two clear-sky days (August 22, 2009 and July 3, 2008) over the entire study area with the MODIS-derived validated LST (MODIS LST). It is noteworthy that more than 70% of the differences between the SEVIRI LST1 and MODIS LST are within 2.5 K; because of the relatively homogeneous thermal conditions of the Earth's surface at night, the differences in LST tend to be lower at night than those during the day. However, further LST and LSE validation work should be conducted using field measurements or other products.

This article has been accepted for inclusion in a future issue of this journal. Content is final as presented, with the exception of pagination.

16   IEEE TRANSACTIONS ON GEOSCIENCE AND REMOTE SENSING

REFERENCES

[1] J. Mallick, Y. Kant, and B. D. Bharath, "Estimation of land surface temperature over Delhi using Landsat-7 ETM+," *J. Ind. Geophys. Union*, vol. 12, no. 3, pp. 131–140, Jul. 2008.

[2] Z.-L. Li, B.-H. Tang, H. Wu, H. Ren, G. J. Yan, Z. Wan, I. F. Trigo, and J. A. Sobrino, "Satellite-derived land surface temperature: Current status and perspectives," *Remote Sens. Environ.*, vol. 131, pp. 14–37, Apr. 2013.

[3] Y. Sun, Retrieval and Application of Land Surface Temperature, 2008, Accessed Jul. 2011. [Online]. Available: http://www.geo.utexas.edu/courses/387h

[4] P. Dash, F. M. Gottsche, F. S. Olesen, and H. Fischer, "Land surface temperature and emissivity estimation from passive sensor data: Theory and practice current trends," *Int. J. Remote Sens.*, vol. 23, no. 13, pp. 2563–2594, Jan. 2002.

[5] J. C. Price, "Estimating surface temperatures from satellite thermal infrared data—A simple formulation for the atmospheric effect," *Remote Sens. Environ.*, vol. 13, no. 4, pp. 353–361, Sep. 1983.

[6] L. M. McMillin, "Estimation of sea surface temperature from two infrared window measurements with different absorptions," *J. Geophys. Res.*, vol. 80, no. C36, pp. 5113–5117, Dec. 1975.

[7] J. C. Price, "Land surface temperature measurements from the split window channels of the NOAA 7 AVHRR," *J. Geophys. Res.*, vol. 89, no. D5, pp. 7231–7237, Aug. 1984.

[8] Z. Wan and J. Dozier, "A generalized split-window algorithm for retrieving land-surface temperature from space," *IEEE Trans. Geosci. Remote*, vol. 34, no. 4, pp. 892–905, Jul. 1996.

[9] C. Coll and V. Caselles, "A split-window algorithm for land surface temperature from advanced very high resolution radiometer data: Validation and algorithm comparison," *J. Geophys. Res.*, vol. 102, no. D14, pp. 16 697–16 713, Jul. 1997.

[10] V. Caselles and J. A. Sobrino, "Determination of frosts in orange groves from NOAA-9 AVHRR data," *Remote Sens. Environ.*, vol. 29, no. 2, pp. 135–146, Aug. 1989.

[11] L. F. Peres and C. C. DaCamara, "Emissivity maps to retrieve land-surface temperature from MSG/SEVIRI," *IEEE Trans. Geosci. Remote*, vol. 43, no. 8, pp. 1834–1844, Aug. 2005.

[12] Z.-L. Li, H. Wu, N. Wang, S. Qiu, J. A. Sobrino, Z. Wan, B.-H. Tang, and G. J. Yan, "Land surface emissivity retrieval from satellite data," *Int. J. Remote Sens.*, vol. 34, no. 9/10, pp. 3084–3127, May 2013.

[13] G. M. Jiang, Z.-L. Li, and F. Nerry, "Land surface emissivity retrieval from combined mid-infrared and thermal infrared data of MSG-SEVIRI," *Remote Sens. Environ.*, vol. 105, no. 4, pp. 326–340, Dec. 2006.

[14] G. M. Jiang, "Retrievals of land surface emissivity and land surface temperature from MSG1-SEVIRI data," Ph.D. dissertation, Univ. Strasbourg, Alsace, France, 2007.

[15] F. Becker and Z.-L. Li, "Towards a local split window method over land surfaces," *Int. J. Remote Sens.*, vol. 11, no. 3, pp. 369–393, Mar. 1990.

[16] F. Becker and Z.-L. Li, "Temperature independent spectral indices in thermal infrared bands," *Remote Sens. Environ.*, vol. 32, no. 1, pp. 17–33, Apr. 1990.

[17] Z. -L. Li and F. Becker, "Feasibility of land surface temperature and emissivity determination from AVHRR data," *Remote Sens. Environ.*, vol. 43, no. 1, pp. 67–85, Jan. 1993.

[18] Z.-L. Li, F. Petitcolin, and R. H. Zhang, "A physically based algorithm for land surface emissivity retrieval from combined mid-infrared and thermal infrared data," *Sci. China Ser. E*, vol. 43, no. Suppl. 1, pp. 23–33, Dec. 2000.

[19] Z. Wan, "New refinements and validation of the MODIS land-surface temperature/emissivity products," *Remote Sens. Environ.*, vol. 112, no. 1, pp. 59–74, Jan. 2008.

[20] Z. Wan and Z.-L. Li, "Radiance-based validation of the V5 MODIS land surface temperature product," *Int. J. Remote Sens.*, vol. 29, no. 17/18, pp. 5373–5395, Sep. 2008.

[21] F. Nerry, F. Petitcolin, and M. P. Stoll, "Bi-directional reflectivity in AVHRR channel 3: Application to a region in North Africa," *Remote Sens. Environ.*, vol. 66, no. 3, pp. 298–316, Dec. 1998.

[22] B. H. Tang, Z.-L. Li, and Y. Y. Bi, "Estimation of land surface directional emissivity in mid-infrared channel approximately 4.0 mm from MODIS data," *Opt. Exp.*, vol. 17, no. 5, pp. 3173–3182, Mar. 2009.

[23] J. L. Roujean, M. Leroy, and P. Y. Deschamps, "A bi-directional reflectance model of the Earth's surface for the correction of remote sensing data," *J. Geophys. Res.*, vol. 97, no. D18, pp. 20 455–20 468, Dec. 1992.

[24] W. Lucht and J. L. Roujean, "Considerations in the parametric modeling of BRDF and albedo from multiangular satellite sensor observations," *Remote Sens. Environ.*, vol. 18, no. 2–4, pp. 343–379, Sep. 2000.

[25] F. M. Göttsche and F. S. Olesen, "Modeling of diurnal cycle of brightness temperature extracted from METEOSAT data," *Remote Sens. Environ.*, vol. 76, no. 3, pp. 337–348, Jun. 2001.

[26] X. Y. Zhang, "Estimation of thermal inertia ground heat flux using geostationary meteorological satellite data," Ph.D. dissertation, Inst. Geograph. Sci. Nat. Resources Res., Chin. Acad. Sci., Beijing, China, 2008.

[27] A. Berk, L. S. Bernstein, G. P. Anderson, P. K. Acharya, D. C. Robertson, J. H. Chetwynd, and S. M. Adler-Golden, "MODTRAN cloud and multiple scattering upgrades with application to AVIRIS," *Remote Sens. Environ.*, vol. 65, no. 3, pp. 367–375, Sep. 1998.

[28] C. X. Gao, B. H. Tang, H. Wu, X. G. Jiang, and Z.-L. Li, "A generalized split-window algorithm for land surface temperature estimation from MSG-2/SEVIRI data," *Int. J. Remote Sens.*, vol. 34, no. 12, pp. 4182–4199, Mar. 2013.

[29] B. H. Tang, Y. Y. Bi, Z.-L. Li, and J. Xia, "Generalized split-window algorithm for estimate of land surface temperature from Chinese geostationary FengYun meteorological satellite (FY-2C) data," *Sensors*, vol. 8, no. 2, pp. 933–951, Feb. 2008.

[30] Z.-L. Li, L. Jia, Z. B. Su, Z. Wan, and R. H. Zhang, "A new approach for retrieving precipitable water from ATSR2 split-window channel data over land area," *Int. J. Remote Sens.*, vol. 24, no. 24, pp. 5059–5117, Dec. 2003.

[31] G. M. Jiang and Z. -L. Li, "Split-window algorithm for land surface temperature estimation from MSG1-SEVIRI data," *Int. J. Remote Sens.*, vol. 29, no. 20, pp. 6067–6074, Oct. 2008.

Caixia Gao received the B.S. degree in electronical and information engineering from the Xi'an University of Posts and Telecommunications, Xi'an, China, the M.S. degree in computer science from the Academy of Opto-Electronics, Chinese Academy of Sciences, Beijing, China, in 2009, and the Ph.D. degree in cartography and geography information system from the University of Chinese Academy of Sciences, Beijing, in 2012.

She is currently an Assistant Researcher of Opto-Electronics with the Chinese Academy of Sciences. Her research interests include the retrieval and validation of surface temperature and emissivities and the intercalibration of satellite sensors.

Zhao-Liang Li received the Ph.D. degree from University of Strasbourg, Strasbourg, France, in 1990.

Since 1992, he has been a Research Scientist with CNRS, Illkirch, France. He joined the Institute of Agricultural Resources and Regional Planning in 2013. He has participated in many national and international projects such as the National Aeronautics and Space Administration (NASA)-funded Moderate Resolution Imaging Spectroradiometer, European Community (EC)-funded program Exploitation of angular effects in land surface observations from satellites (EAGLE), and ESA-funded programs SPECTRA, etc. His main expertise fields are in thermal infrared radiometry, parameterization of land surface processes at large scale, and assimilation of satellite data to land surface models. He has published more than 100 papers in international refereed journals.

Shi Qiu is currently working toward the Ph.D degree at CNRS, Illkirch, France. Her research interest includes the land surface temperature retrieval from passive microwave remote sensing.

Bohui Tang received the B.S. degree in cartography and Geographic Information System (GIS) from the Wuhan Technical University of Surveying and Mapping, Wuhan, China, in 1999 and the M.S. degree and the Ph.D. degree in quantitative remote sensing from the Graduate University of Chinese Academy of Sciences, Beijing, China, in 2004 and 2007, respectively.

He is currently working as a Quantitative Remote Sensing Specialist with the Institute of Geographic Sciences and Natural Resources Research, Chinese Academy of Sciences, Beijing. His present research interests focus on the quantitative estimation of land surface variables from satellite remote sensing, surface net radiation estimation from satellite data, and remote sensing applications for cryosphere monitoring and assessment. He has published more than 30 papers in international refereed journals.

Hua Wu received the B.S. degree in photogrammetric engineering and remote sensing from Wuhan University, Wuhan, China, in 2003, the M.S. degree in cartography and geographical information system from Beijing Normal University, Beijing, China, in 2006, and the Ph.D. degree in cartography and geographical information system from the Institute of Geographic Sciences and Natural Resources Research, Chinese Academy of Sciences, Beijing, in 2010.

He is currently a Research Assistant with the Institute of Geographic Sciences and Natural Resources Research, Chinese Academy of Sciences. His research mainly includes the retrieval and validation of surface temperature and emissivities and the scaling of remotely sensed products.

Xiaoguang Jiang received the Ph.D. degree in remote sensing and GIS from the Institute of Remote Sensing Applications, Chinese Academy of Sciences (CAS), Beijing, China, in 2000.

He is currently a Professor with the University of Chinese Academy of Sciences, Beijing. Since 1987, he has been always working on remote sensing data processing, land surface parameter retrieval, and validation of remote sensing and participated more than 30 so-called National High Technology Development Plan (863 Plan) projects, National Key Projects, Projects from National Natural Science Foundation of China, Projects of Knowledge Innovation of CAS, international cooperation projects, etc. He published more than 60 research papers and copublished two research books.